CrystEngComm

For Table of Contents Use Only

Table of Contents Graphic and Synopsis

Mixed-Solvent/Metal/pH/-Dependent Structural Variations Based on C_2-Symmetric 2,6-Bis(3,5-dicarboxylphenyl)pyridine Ligand: Solvothermal Syntheses, Structural Characterizations, and Magnetic Properties

Liming Fan, Weiliu Fan, Bin Li, Xinzheng Liu, Xian Zhao and Xiutang Zhang

Five coordination polymers, featuring 2D wave sheet, and 3D (3,5), (4,6), (3,4,5), and (4,4,8)-connected nets, have been assembled from the 2,6-bis(3,5-dicarboxylphenyl)pyridine by systematically tuning the ratios of mixed solvent and pH values.
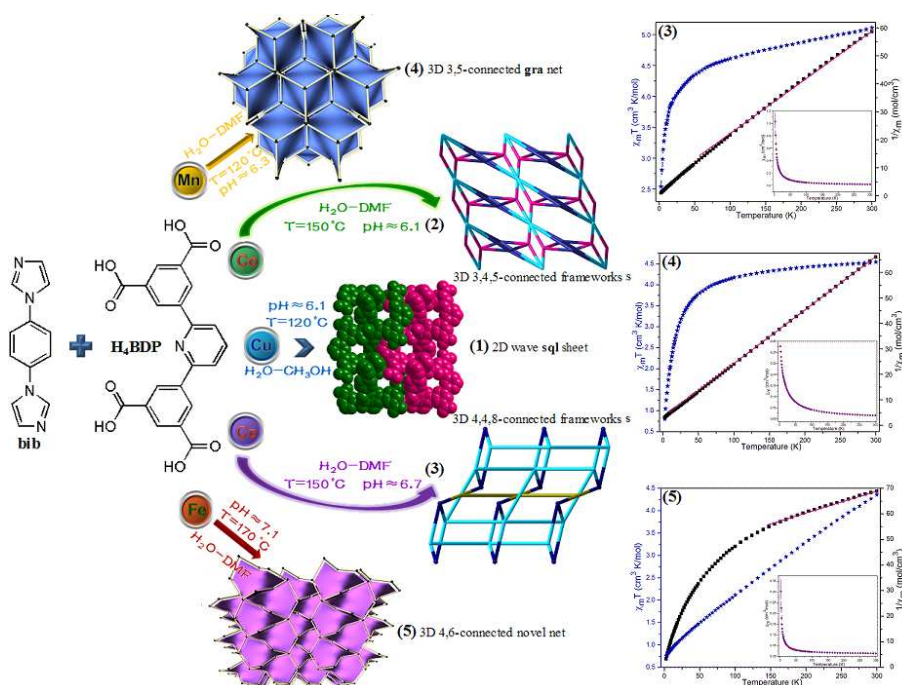
CrystEngComm

Cite this: DOI: 10.1039/c5ce00000x

www.rsc.org/CrystEngComm

ARTICLE

Mixed-Solvent/Metal/pH/-Dependent Structural Variations Based on C_2-Symmetric 2,6-Bis(3,5-dicarboxylphenyl)pyridine Ligand: Solvothermal Syntheses, Structural Characterizations, and Magnetic Properties

Liming Fan,[a,b] Weiliu Fan,[a] Bin Li,[b] Xinzheng Liu,[b] Xian Zhao*[a] and Xiutang Zhang*[a,b]

5

ABSTRACT: Five new coordination polymers (CPs) with distinct structures and topologies, namely, $\{[Cu(H_2BDP)(bib)]_{0.5} \cdot H_2O\}_n$ (1), $\{[Co_{1.5}(HBDP)(bib)_2(H_2O)] \cdot 3H_2O\}_n$ (2), $\{[Co_2(BDP)(bib)_2] \cdot H_2O\}_n$ (3), $\{[Mn(BDP)_{0.5}(bib)_{1.5}(\mu_2\text{-}H_2O)_{0.5}(H_2O)] \cdot 0.5H_2O\}_n$
10 (4), and $\{[Fe_2(BDP)(bib)(H_2O)] \cdot H_2O\}_n$ (5) (H_4BDP = 2,6-bis(3,5-dicarboxyphenyl)pyridine, bib = 1,4-bis(imidazol-1-yl)benzene), have been synthesized by systematically tuning the ratios of mixed solvent and pH values. Along with the altering ratios of the mixed-solvent DMF/H_2O or CH_3OH/H_2O used in the synthetic processes, the coordination modes of the ligand change, which further lead to the different structures of resultant complexes. Owing to diverse metal centers and distinct ligand coordination modes, these five complexes exhibit totally diverse structures. Complex 1 displays a 2D 4-connected $(4^4.6^2)$-**sql** wave-like sheet, which is further
15 expanded to a 3D supramoelcular structure *via* the $\pi\cdots\pi$ interactions. In complex 2, 1D $[Co(bib)]_n$ straight chains and 1D $[Co_2(bib)_3]_n$ ladder-like chains interacted each other to form a 2D net, which are linked by $HBCP^{3-}$ ligands to generate a 3D (3,4,5)-connected $(4^2 \cdot 6^4 \cdot 7^3 \cdot 9)_2(6^2 \cdot 7)_2(6^4 \cdot 7 \cdot 8)$ architecture. Complex 3 exhibits an unprecedented 3D (4,4,8)-connected net with the Schläfli symbol of $(3 \cdot 4^2 \cdot 5^2 \cdot 6)_4(3^2 \cdot 4^4 \cdot 5^4 \cdot 6^4 \cdot 7^2 \cdot 8^6 \cdot 9^5 \cdot 10)$. Complex 4 exhibits a dinuclear $\{Mn_2(\mu_2\text{-}H_2O)\}$ based 3D (4,8)-connected $(6^3)(6^9 \cdot 8)$-**gra** framework. For complex 5, the whole structure can be regard as a $\{Fe_2(COO)_4\}$ binuclear SBUs based
20 3D architecture with (4,6)-connected $(4^4 \cdot 6^{10} \cdot 8)(4^4 \cdot 6^2)$ topology. Besides, the magnetic properties of complexes 3–5 have been investigated.

Introduction

The crystalline functional coordination polymers (CPs), as a prominent representative of inorganic-organic hybrid materials, have attracted more and more research interest, not only for their interesting topologies but also for their potential applications in many fields, such as new energy, industrial catalysis, information storage, electronic devices, drug delivery.[1-4] Up to now, the design and syntheses of functional CPs is still a huge challege, because the reaction conditions as well as the nature of selected organic ligands have great influences on the crystal growth.[5-7]

Despite the breathtaking achievements in this aspect, however, to predict and further accurately control the framework array of a given crystalline product remain a considerable challenge at this stage. This mainly arises from the fact that the subtle assembled progress may be influenced by many intrinsic and external parameters, such as the different coordination preferences of metal ion, templating

agents, metal-ligand ratio, pH value, anions, and number of coordination sites provided by organic ligands.[8,9] Among these factors, the rational selection of organic ligands or coligands according to their length, rigidity and functional groups is important for the assembly of structural controllable CPs, and a great deal of significant works have been done by using this strategy.[10] Usually, organic ligands with bent backbones, such as V-shaped, triangular, quadrangular, and so on, are excellent candidates for building highly high-connected, interpenetrating, or helical coordination frameworks due to their bent backbones and versatile bridging fashions.[11] In addition, carboxylate groups are good hydrogen-bond acceptors as well as donors, depending upon the degree of deprotonation. Among which, quadrangular polycarboxylic acids, such as 1,3-di((2',4'-dicarboxylphenyl)benzene, 3,3″,5,5″-terphenyltetracarboxylic acid, 2,2″,5,5″-terphenyltetracarboxylic acid, are paid much attention due to their rich coordination modes.[12-14] Apart from the carboxylate linkers, bis(triazole) and bis(imidazole) bridging ligands with different lengths and flexibilities, such as 1,4-bis(1,2,4-triazol-1-ylmethyl)benzene (btx), 1,4-bis(imidazol-1-ylmethyl)benzene, 4,4′-bis(imidazol-1-yl)biphenyl, and 4,4′-bis(imidazol-1-ylmethyl)biphenyl are frequently used in the assembly process of CPs as bridging linkers, guest molecules, or charge balance roles.[15]

Based on the above mentioned points and our recent research,

[a] *State Key Laboratory of Crystal Materials, Shandong University , Jinan 250100, China. E-mail: zhaoxian@sdu.edu.cn.*
[b] *Advanced Material Institute of Research, College of Chemistry and Chemical Engineering, Qilu Normal University, Jinan, 250013, China. E-mail: xiutangzhang@163.com.*

2,6-bis(3,5-dicarboxyphenyl)pyridine (H$_4$BDP) and 1,4-bis(imidazol-1-yl)benzene (bib) were employed to react with transition metal ions under solvothermal conditions. Herein, we reported the syntheses and characterizations of five new CPs, {[Cu(H$_2$BDP)(bib)]$_{0.5}$·H$_2$O}$_n$ (**1**), {[Co$_{1.5}$(HBDP)(bib)$_2$(H$_2$O)]·3H$_2$O}$_n$ (**2**), {[Co$_2$(BDP)(bib)$_2$]·H$_2$O}$_n$ (**3**), {[Mn(BDP)$_{0.5}$(bib)$_{1.5}$(μ_2-H$_2$O)$_{0.5}$(H$_2$O)]·0.5H$_2$O}$_n$ (**4**), and {[Fe$_2$(BDP)(bib)(H$_2$O)]·H$_2$O}$_n$ (**5**). Structural analyses showed that the H$_4$BDP ligands took on five different coordination modes in the five CPs and thus resulted in diverse structures, which exhibit a systematic variation of architectures from 2D 4-connected wave **sql** sheet (**1**), 3D (3,5)-connected **gra** net (**4**), 3D (4,6)-connected $(4^4·6^{10}·8)(4^4·6^2)$ net (**5**), 3D (3,4,5)-connected $(4^2·6^4·7^3·9)_2(6^2·7)_2(6^4·7·8)$ net (**2**), to 3D (4,4,8)-connected $(3·4^2·5^2·6)_4(3^2·4^4·5^4·6^4·7^2·8^6·9^5·10)$ net (**3**) (Scheme 1). These results revealed that the reaction conditions, including the metal ions, the mixed solvents, as well as the pH, have great influence on the final structures.
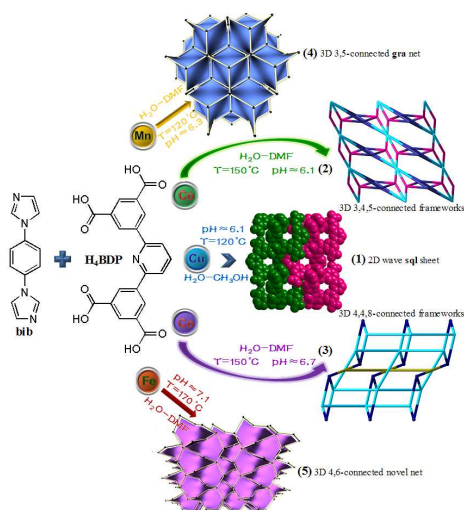
Scheme 1. Structural diversity of the obtained CPs.

Experimental Section

Materials and Methods. 2,6-bis(3,5-dicarboxyphenyl)pyridine (H$_4$BDP) and 1,4-bis(imidazol-1-yl)benzene (bib) were purchased from Jinan Henghua Sci. & Tec. Co. Ltd. without further purification. IR spectra were measured on a NEXUS 670 FTIR spectrometer at the range of 600-4000 cm^{-1}. Elemental analyses were carried out on a CE instruments EA 1110 elemental analyzer. TGA was measured from 25 to 800 °C on a SDT Q600 instrument at a heating rate 5 °C/min under the N$_2$ atmosphere (100 mL/min). X-ray powder diffractions were measured on a Panalytical X-Pert pro diffractometer with Cu-Kα radiation. The variable-temperature magnetic susceptibility measurements were performed on the Quantum Design SQUID MPMS XL-7 instruments in the temperature range of 2-300 K under a field of 1000 Oe.

General Synthesis Procedure for Complexes 1–5. Five title compounds were synthesized under hydrothermal conditions and their formation were strongly influenced by reaction conditions such as metal ions, temperature, pH, and the ration of solvents,

which play an important role on adjusting the coordination modes of H$_4$BDP as well as the final crystal packing structures. To check the phase purity of **1−5**, PXRD has been introduced. The comparisons of measured and simulated PXRD patterns shows the main peaks are aligned with each other, which indicated the high purity of those complexes (Fig. S1). For **1−5**, the IR absorption bands around 3450 cm^{-1} can be attributed to the characteristic peaks of O-H vibrations. The vibrations at about 1400 cm^{-1} and 1610 cm^{-1} correspond to the asymmetric and symmetric stretching vibrations of the carboxyl groups, respectively (Fig. S2).[16]

Synthesis of {[Cu(H$_2$BDP)(bib)]$_{0.5}$·H$_2$O}$_n$ (1). A mixture of H$_4$BDP (0.10 mmol, 0.041 g), bib (0.30 mmol, 0.063 g), CuSO$_4$·5H$_2$O (0.20 mmol, 0.050 g), 6 mL H$_2$O and 3 mL methanol was sealed in a 25 mL Teflon-lined stainless steel vessel, which was heated to 120 °C for 3 days and then cooled to 25 °C at a rate of 0.5 °C min^{-1}. Blue-purple block crystals of **1** were obtained. Yield 40% based on H$_4$BDP. Anal. (%) calcd. for C$_{33}$H$_{23}$CuN$_5$O$_{10}$: C, 55.58; H, 3.25; N, 9.82. Found: C, 55.62; H, 3.37; N, 9.71. IR (KBr pellet, cm^{-1}): 3116 (s), 2378 (s), 2115 (s), 1705 (s), 1650 (m), 1610 (m), 1568 (s), 1526 (vs), 1399 (s), 1355 (m), 1243 (m),1068 (m), 834 (m), 741 (w).

Synthesis of {[Co$_{1.5}$(HBDP)(bib)$_2$(H$_2$O)]·3H$_2$O}$_n$ (2). A mixture of H$_4$BDP (0.15 mmol, 0.061 g), bib (0.30 mmol, 0.063 g), CoCl$_2$·6H$_2$O (0.30 mmol, 0.071 g), 12 mL H$_2$O and 2 mL DMF was sealed in a 25 mL Teflon-lined stainless steel vessel, which was heated to 150 °C for 3 days and then cooled to 25 °C at a rate of 0.5 °C min^{-1}. Red block crystals of **2** were obtained. Yield 53% based on H$_4$BDP. Anal. (%) calcd. for C$_{90}$H$_{76}$Co$_3$N$_{18}$O$_{24}$: C, 62.42; H, 3.24; N, 10.65. Found: C, 61.74; H, 3.31; N, 10.70. IR (KBr pellet, cm^{-1}): 3443 (w), 3372 (w), 2918 (vs), 2850 (vs), 1718 (w), 1629 (w), 1569 (w), 1528 (m), 1464 (m), 1066 (m), 780 (w), 719 (w).

Synthesis of {[Co$_2$(BDP)(bib)$_2$]·H$_2$O}$_n$ (3). A mixture of H$_4$BDP (0.15 mmol, 0.061 g), bib (0.30 mmol, 0.063 g), CoCl$_2$·6H$_2$O (0.30 mmol, 0.071 g), NaOH (0.20 mmol, 0.008 g), 12 mL H$_2$O and 2 mL DMF was sealed in a 25 mL Teflon-lined stainless steel vessel, which was heated to 150 °C for 3 days and then cooled to 25 °C at a rate of 0.5 °C min^{-1}. Purple block crystals of **3** were obtained with the yield of 62% (based on H$_4$BDP). Anal. (%) calcd. for C$_{45}$H$_{29}$Co$_2$N$_9$O$_9$: C, 56.44; H, 3.05; N, 13.16. Found: C, 56.11; H, 3.23; N, 12.98. IR (KBr pellet, cm^{-1}): 3439 (w), 3127 (m), 1622 (m), 1568 (m), 1527 (vs), 1397 (s), 1342 (m), 1307 (s), 1066 (m), 836 (m), 775(m), 724 (m), 653 (w).

Synthesis of {[Mn(BDP)$_{0.5}$(bib)$_{1.5}$(μ_2-H$_2$O)$_{0.5}$(H$_2$O)]·0.5H$_2$O}$_n$ (4). A mixture of H$_4$BDP (0.15 mmol, 0.061 g), bib (0.30 mmol, 0.063 g), MnSO$_4$·H$_2$O (0.30 mmol, 0.051 g), NaOH (0.20 mmol, 0.008 g), 6 mL H$_2$O and 3 mL DMF was sealed in a 25 mL Teflon-lined stainless steel vessel, which was heated to 120 °C for 3 days and then cooled to 25 °C at a rate of 0.5 °C min^{-1}. Colorless crystals of **4** were obtained. Yield 38% based on H$_4$BDP. Anal. (%) calcd. for C$_{57}$H$_{47}$Mn$_2$N$_{13}$O$_{12}$: C, 56.30; H, 3.90; N, 14.98. Found: C, 56.06; H, 4.02; N, 14.97. IR (KBr pellet, cm^{-1}): 3132 (vs), 2112 (m), 1988 (w), 1616 (s), 1552 (m), 1530 (s), 1442 (m), 1338 (m), 1304 (m), 1252 (m), 1066 (s), 830 (m), 627 (s).

Synthesis of {[Fe$_2$(BDP)(bib)(H$_2$O)]·H$_2$O}$_n$ (5). A mixture

of H_4BDP (0.15 mmol, 0.061 g), bib (0.30 mmol, 0.063 g), $FeSO_4 \cdot 7H_2O$ (0.30 mmol, 0.084 g), NaOH (0.20 mmol, 0.008 g), 14 mL H_2O and 2 mL DMF was sealed in a 25 mL Teflon-lined stainless steel vessel, which was heated to 170 °C for 3 days and then cooled to 25 °C at a rate of 0.5 °C min^{-1}. Red block crystals of **5** were obtained with 44% yield (based on H_4BDP). Anal. (%) calcd. for $C_{33}H_{23}Fe_2N_5O_{10}$: C, 52.07; H, 3.05; N, 9.20. Found: C, 52.36; H, 3.31; N, 9.21. IR (KBr pellet, cm^{-1}): 3471 (w), 3129 (w), 1604 (m), 1570 (s), 1528 (vs), 1435 (m), 1399 (s), 1347 (s), 1307 (s), 1066 (m), 776 (m), 726 (m), 654 (m).

X-ray crystallography. Intensity data collection was carried out on a Siemens SMART diffractometer equipped with a CCD detector using Mo-$K\alpha$ monochromatized radiation ($\lambda = 0.71073$ Å) at 296(2) K. The absorption correction was based on multiple and symmetry-equivalent reflections in the data set using the SADABS program based on the method of Blessing. The structures were solved by direct methods and refined by full-matrix least-squares using the SHELXTL package.[17] All non-hydrogen atoms were refined anisotropically. Hydrogen atoms except those on water

molecules were generated geometrically with fixed isotropic thermal parameters, and included in the structure factor calculations. The hydrogen atoms attached to oxygen were refined with O–H=0.85Å and $U_{iso}(H) = 1.2U_{eq}(O)$. The lattice water molecules in complexes **1**, **2** and **5** are disordered and refined with the occupancy ratio of 50:50 for O(1W) and O(1WA) in complex **1**; 50:50 for O(3W) and O(3WA), 40:40:20 for O(4W), O(4WA) and O(4WB) in complex **2**; 50:50 for O(2W) and O(2WA) in complex **5**, respectively. Besides, all the hydrogen atoms attached the disordered lattice water molecules are omitted for clarity. Crystallographic data for complexes **1–5** are given in Table 1. Selected bond lengths and angles for **1–5** are listed in Table S1. For complexes of **1–5**, further details of the crystal structure can be obtained from the http://www.ccdc.cam.ac.uk/deposit, on quoting the depository number CCDC-1042873 for **1**, 1042874 for **2**, 1042875 for **3**, 1042876 for **4**, and 1042872 for **5**. Topological analysis of the coordination networks of all the compounds was performed with the program package TOPOS.[18]

Table 1 Crystal data for **1–5**

Compound	1	2	3	4	5
Empirical formula	$C_{33}H_{25}CuN_5O_{10}$	$C_{90}H_{76}Co_3N_{18}O_{24}$	$C_{45}H_{31}Co_2N_9O_9$	$C_{57}H_{47}Mn_2N_{13}O_{12}$	$C_{33}H_{23}Fe_2N_5O_{10}$
Formula weight	715.13	1970.47	959.65	1215.96	761.25
Crystal system	Monoclinic	Monoclinic	Monoclinic	Monoclinic	Triclinic
Space group	$P2/n$	$C2/c$	$P2_1/n$	$C2/c$	$P-1$
a (Å)	7.6476(5)	24.5299(12)	10.898(2)	17.6549(9)	9.6476(6)
b (Å)	12.1053(7)	12.3443(6)	12.605(3)	16.6017(7)	10.2117(7)
c (Å)	16.8248(10)	31.5597(15)	28.807(6)	19.0614(9)	16.4488(11)
α (°)	90	90	90	90	107.3660(10)
β (°)	98.488(2)	100.3370(10)	96.326(4)	112.771(2)	95.2210(10)
γ (°)	90	90	90	90	99.9140(10)
$V(Å^3)$	1540.52(16)	9401.3(8)	3932.9(15)	5151.5(4)	1505.97(17)
Z	2	4	4	4	2
D_{calcd} (Mg/m^3)	1.533	1.384	1.621	1.568	1.674
μ(mm^{-1})	0.778	0.606	0.918	0.572	1.035
R_{int}	0.1015	0.0303	0.0421	0.0455	0.0165
Final R indices[$I > 2\sigma(I)$]^a	$R_1 = 0.0645$, $wR_2 = 0.1411$	$R_1 = 0.0549$ $wR_2 = 0.1671$	$R_1 = 0.0412$, $wR_2 = 0.1040$	$R_1 = 0.0367$, $wR_2 = 0.0859$	$R_1 = 0.0331$, $wR_2 = 0.0931$
R indices (all data)^a	$R_1 = 0.0911$, $wR_2 = 0.1531$	$R_1 = 0.0682$, $wR_2 = 0.1804$	$R_1 = 0.0628$, $wR_2 = 0.1243$	$R_1 = 0.0457$, $wR_2 = 0.0910$	$R_1 = 0.0370$, $wR_2 = 0.0959$
Gof	1.108	1.107	1.084	1.045	1.043

$^a R_1 = \Sigma| |F_o|-|F_c| |/ \Sigma|F_o|, wR_2 = [\Sigma w(F_o^2-F_c^2)^2]/ \Sigma w(F_o^2)^2]^{1/2}$

Result and Discussion

Structural Description of $\{[Cu(H_2BDP)(bib)]_{0.5} \cdot H_2O\}_n$ (1). Structural analysis reveals that Cu^{II} ions are bridged by H_2BDP^{2-} to form snake-like chains, which are further linked by bib to generate a 2D parallel entangled sheet. Complex **1** crystallizes in the monoclinic system, space group $P2/n$. As shown in Fig. 1a, the asymmetric unit consists of one half Cu^{II} ion, one half bib ligand and one half BDP ligand, and one lattice water molecule. Each Cu^{II} ion lies on an inversion centre, tetra-coordinated by two carboxylate O atoms from two H_2BDP^{2-}ligands and two N atoms from two bib ligands.

In **1**, H_4BDP is partially deprotonated and acts as bidentate ligand with C_2-symmetric axis (Mode I, Scheme 2). Cu^{II} ions are connected by H_2BDP^{2-} to form snake-like $[Cu(H_2BDP)]_n$ chains with the nearest Cu⋯Cu distance being 8.711 Å (Fig. 1b), which are further bridged by bib ligands to generate a 2D wave sheet (Fig. 1c). Topology analysis shows that the overall network of **1** can be defined as a 4–connected $(4^4 \cdot 6^2)$–**sql** layer by denoting the

H_2BDP^{2-} and bib ligands as bridging linkers, and Cu^{II} ions as 4–connected nodes, respectively. It is also noteworthy that the neighbouring sheets interacted with each other through the π⋯π interactions [Cg–Cg = 3.565 Å] between phenyl rings, finally exhibiting a 3D supramolecular structure (Fig. 1d and Fig. S3).

Structural Description of $\{[Co_{1.5}(HBDP)(bib)_2(H_2O)] \cdot 3H_2O\}_n$ (2). X-ray diffraction analysis reveals that complex **2** crystallizes in the monoclinic system, space group $C2/c$. As shown in Fig. 2a, the asymmetric unit of **2** consists of one and a half Co^{II} ions, one partly deprotonated $HBDP^{3-}$ ligand, two bib ligands, one associated water molecule, and three lattice water molecules. Co(1) atom is in a general position of the slightly distorted $\{CoN_3O_3\}$ octahedral geometry, surrounded by three O atoms from two different $HBDP^{3-}$ ligands and three N atoms from three bib ligands. While Co(2) atom locates in an inversion centre of the $\{CoN_2O_4\}$ octahedral geometry, completed by four O atoms from two distinct BDP^{4-} ligands and two coordinated water molecules, and two N atoms from two bib ligands.

Different from that in complex **1**, the H$_4$BDP exhibits (κ^1-κ^0)-(κ^1-κ^1)-(κ^1-κ^0)-μ_3 coordination mode (Mode II) in **2** with one carboxyl group protonated. Each HBDP^{3-} ligand linked two Co(1) and one Co(2) ions through two monodentate (κ^0-κ^1)-μ_1 and one cheating (κ^1-κ^1)-μ_1 carboxyl groups, successfully generating a 2D [Co$_3$(HBDP)$_2$] sheet (Fig. S4). And then the 2D sheets are further linked by bib ligands with *trans*- configuration to generate a 3D framework (Fig. 2c). From another perspective, Co^{II} ions are bridged by bib ligands to form a 2D [Co(bib)$_2$]$_n$ layer with square circles (Fig. 2b).

From the viewpoint of topology, the final structure of **2** can be defined as an unprecedented (3,4,5)-connected net with the Schläfli symbol of $(4^2 \cdot 6^4 \cdot 7^3 \cdot 9)_2 (6^2 \cdot 7)_2 (6^4 \cdot 7 \cdot 8)$ by denoting HBDP^{3-}, Co(1), and Co(2) as 3–connected nodes, 5–connected, and 4–connected nodes, respectively (Fig. 2d).
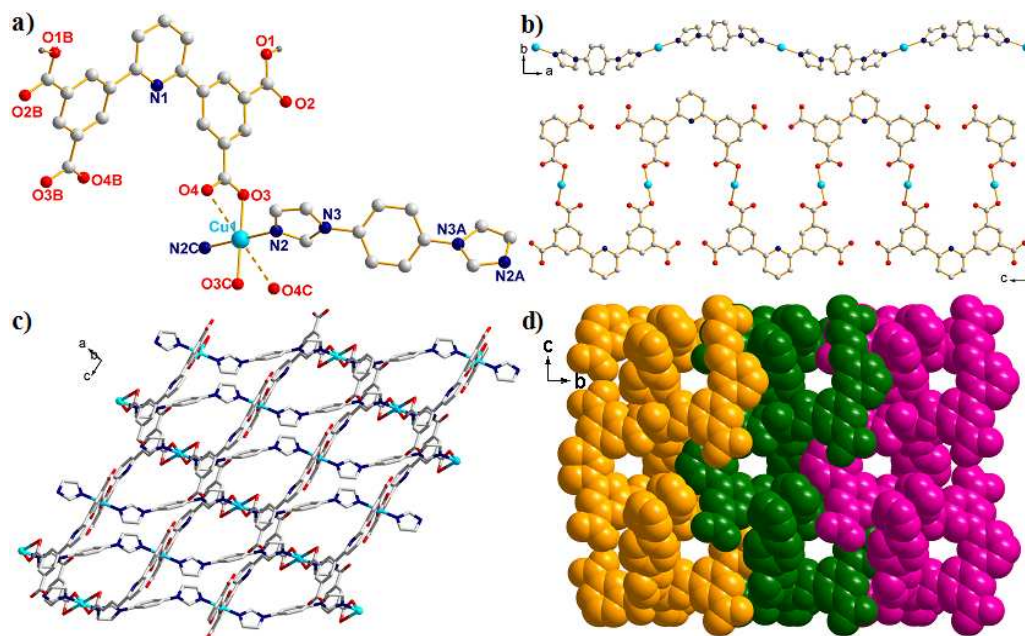
Figure 1. (a) Crystal structure of complex **1** (Symmetry codes: A: 5/2–*x*, *y*, 1/2–*z*; B: 1/2–*x*, *y*, –1/2–*z*; C: 1–*x*, 2–*y*, –*z*). (b) The 1D wave [Cu(bib)]$_n$ chain (the above) and [Cu(H$_2$BDP)]$_n$ snake chain (the below). (c) Schematic view of the 2D sheet of **1**. (d) The 3D packing structures of **1** view along *a* direction.
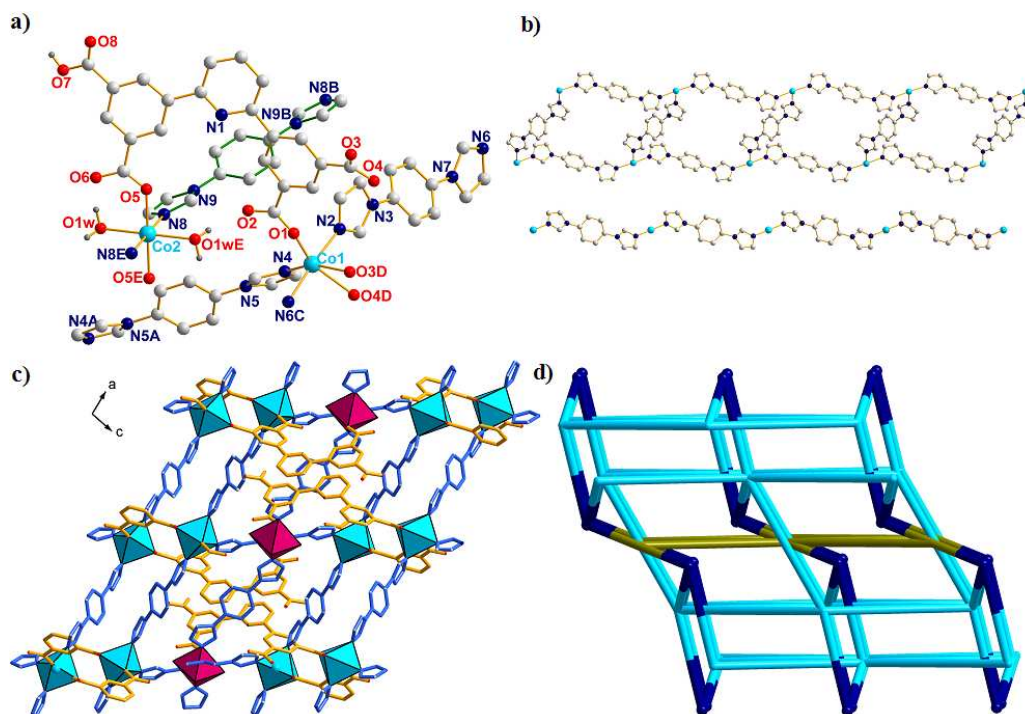
Figure 2. (a) Crystal structure of complex **2** (Symmetry codes: A: 1–*x*, –*y*, 1–*z*; B: 1/2–*x*, 1/2–*y*, 1–*z*; C: 1/2+*x*, 1/2+*y*, *z*; D: 1/2–*x*, –1/2+*y*, 1/2–*z*; E: 1–*x*, 1–*y*, 1–*z*.). (b) The 1D [Co$_2$(bib)$_3$]$_n$ ladder chain (the above) and [Co(bib)]$_n$ straight chain (the below). (c) Schematic view of the 3D frameworks of **2** along

b direction (green spheres: Co(1) ions, red spheres: Co(2) ions). (d) The 3D novel (3,4,5)–connected $(4^2 \cdot 6^4 \cdot 7^3 \cdot 9)_2 (6^2 \cdot 7)_2 (6^4 \cdot 7 \cdot 8)$ topology of **2** (green spheres: Co(1) ions, brown spheres: Co(2) ions; dark blue spheres: HBDP $^{3-}$ ligands).
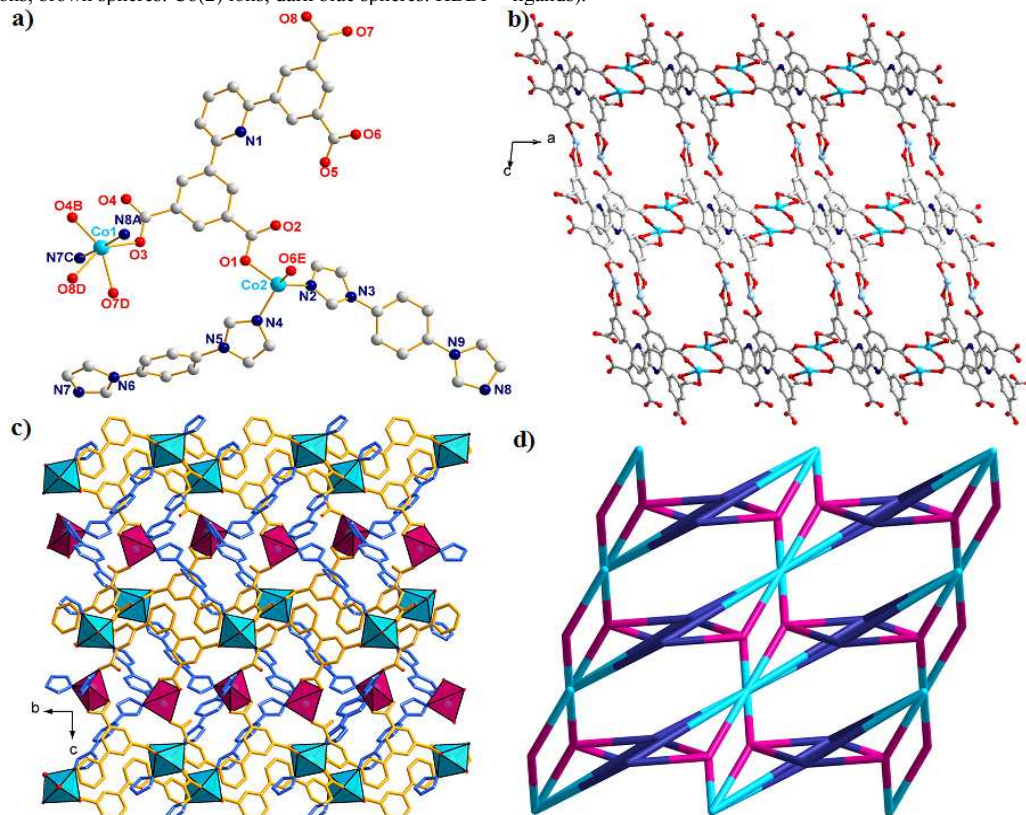
Figure 3. (a) Crystal structure of complex **3** (Symmetry codes: A:1/2-*x*, 1/2+*y*, 3/2-*z*; B: -1-*x*, 2-*y*, 1-*z*; C: -1-*x*, 1-*y*, 1-*z*; D:-1+*x*, -1+*y*, *z*; E: 1/2-*x*, -1/2+*y*, 3/2-*z*.). (b) The 3D porous [Co₂(BDP)]ₙ frameworks view along *b* direction. (c) Schematic view of the 3D frameworks of **3** along *a* direction (green spheres: Co(1) ions, red spheres: Co(2) ions). (d) The 3D novel (4,4,8)–connected $(3 \cdot 4^2 \cdot 5^2 \cdot 6)_4 (3^2 \cdot 4^4 \cdot 5^4 \cdot 6^4 \cdot 7^2 \cdot 8^6 \cdot 9^5 \cdot 10)$ topology of **3** (green spheres: {Co₂(COO)₂} clusters based SBUs, dark blue spheres: Co(2) ions; red spheres: BDP $^{4-}$ ligands).
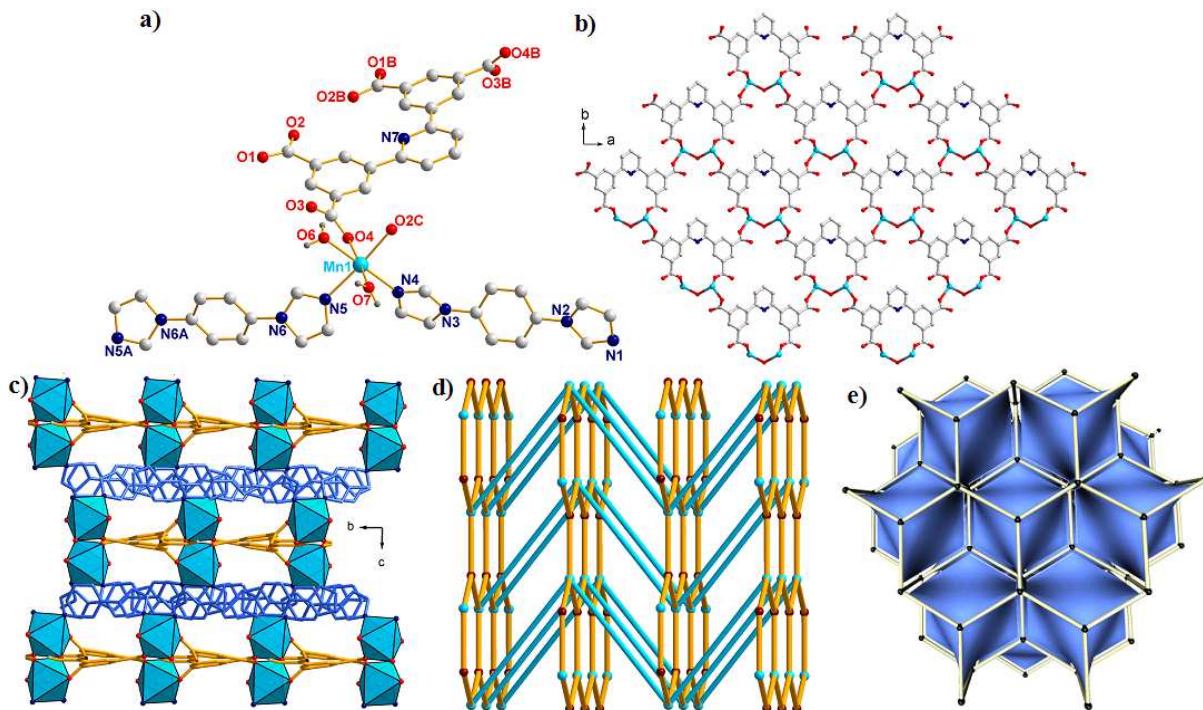
Figure 4. (a) Crystal structure of complex **4** (Symmetry codes: A: –*x*, 1–*y*, 1–*z*; B: 1–*x*, *y*, 1/2–*z*; C: 1/2–*x*, 1/2+*y*, 1/2–*z*.). (b) The 2D [Mn₂(BDP)(H₂O)]ₙ network view along *c* direction. (c) Schematic view of the 3D frameworks of **4** along *a* direction. (d) The 3D (4,8)–connected $(6^3)(6^9 \cdot 8)$-**gra** net of **4** (green spheres: {Mn₂(COO)₄(H₂O)} clusters based SBUs, dark red spheres: BDP $^{4-}$ ligands). (e) Topological features of **4** displayed by tiling style.

Structural Description of {[Co₂(BDP)(bib)₂]·H₂O}ₙ (3). With NaOH being employed in the reaction, H₄BDP in **3** is completely deprotonated. Complex **3** crystallizes in the monoclinic system, space group $P2_1/n$. The asymmetric unit consists of two Co^{II} ions, one BDP^{4-}, two bib, and one lattice water molecule (Fig. 3a). Co (1) is hexacoordinated by four O atoms from three different BDP^{4-} ligands and two N atoms from two different bib linkers, exhibiting a slightly distorted octahedral geometry. Co (2) is tetracoordinated by two O atoms from two BDP^{4-} ligands and two N atoms from two bib ligands.

BDP^{4-} exhibits $(\kappa^0-\kappa^1)-(\kappa^1-\kappa^1)-(\kappa^1-\kappa^1)-(\kappa^1-\kappa^1)-\mu_5$ coordination mode (Mode III) and coordinates to five cobalt ions to form a 3D $[Co_2(BDP)]_n$ framework with 1D channels with 14.261(4) × 10.680(2) Å^2 pores along b axis (Fig. 3b). The ligands of bib occupied those 1D channels via connecting adjacent Co^{II} ions, finally exhibiting 3D net with 1D helix chains (Fig. 3c and Fig. S5). The dihedral angle between two phenyl rings and central pyridine ring in BDP^{4-} are 26.4(1) and 10.6(6)°, respectively. And the one between two phenyl rings in one BDP^{4-} is 22.8(4)°. This dihedral data indicates that the BDP^{4-} was extremely unsymmetrical due to that each carboxylate group participates in coordination to metal ions.

Topology analysis reveals that complex **3** can be rationalized to a (4,4,8)-connected net with the Schläfli symbol of $(3\cdot4^2\cdot5^2\cdot6)_4(3^2\cdot4^4\cdot5^4\cdot6^4\cdot7^2\cdot8^6\cdot9^5\cdot10)$ by denoting Co(2) and BDP^{4-} as 4–connected nodes, and {Co₂(COO)₂} SBUs as 8–connected nodes (Fig. 3d).

Structural Description of {[Mn(BDP)₀.₅(bib)₁.₅(μ₂-H₂O)₀.₅(H₂O)]·0.5H₂O}ₙ (4). Structural analysis reveals that complex **4** crystallizes in the monoclinic system $C2/c$. As shown in Fig. 4a, there are one crystallographically independent Mn^{II} ion, a half BDP^{4-} ligand which lies on a twofold axis, one and a half of bib ligands, one and a half of coordinated water molecules, and a half of lattice water molecule in the asymmetric unit. Mn^{II} is hexacoordinated by two N atoms from two bib ligands, and

four O atoms from two BDP^{4-} ligands and two coordinated water molecules, exhibiting distorted octahedral coordination geometry.

The BDP^{4-} ligand is C_2-symmetric and exhibits $(\kappa^1-\kappa^0)-(\kappa^1-\kappa^0)-(\kappa^1-\kappa^0)-(\kappa^1-\kappa^0)-\mu_4$ coordination mode (Mode IV) to link four metal ions. The dihedral angles between two phenyl rings and central pyridine ring in BDP^{4-} are equal (7.1(5)°). And the one between two phenyl rings is in BDP^{4-} is 13.7(9)°. This dihedral data indicates that the distortion of BDP^{4-} is smaller than the one in **3**. Each two Mn^{II} ions are linked by one μ_2-H₂O to form {Mn₂(μ_2-H₂O)} SBUs, which are further bridged by four carboxylate groups from four BDP^{4-} ligands to generate 2D $[Mn_2(BDP)(H_2O)]_n$ layers (Fig. 4b), which are extended to a 3D framework (Fig. 4c). It is also worthy to note that two kinds of bib ligands exist: one is in a general position and acts as a monodentate ligand, while another lies on an inversion centre and acts as a μ_2 bridge. Mn^{II} ions are coordinated by the two kinds of bib ligands to form a Mn₂(bib)₃ trimer (Fig. S6). From the viewpoint of structural topology, the whole structure of complex **4** can be defined as a (4,8)–connected **gra** net with the Schläfli symbol of $(6^3)(6^9\cdot8)$ by denoting the {Mn(COO)₄(H₂O)} binuclear SBUs to 8–connected nodes and BDP^{4-} ligands to 4–connected nodes, respectively (Fig. 4d and 4e).

Structural Description of {[Fe₂(BDP)(bib)(H₂O)]·H₂O}ₙ (5). Structural analysis reveals that complex **5** is a {Fe₂(COO)₄} binuclear SBUs based 3D framework, crystallizes in the triclinic system, space group P-1. As shown in Fig. 5a, there are two crystallographically independent Fe^{II} ions, one BDP^{4-} ligand, two half bib ligands which both lying about independent inversion centres, one coordinated and one lattice water molecules in the asymmetric unit. Fe (1) is pentacoordinated with five O atoms from three different BDP^{4-} ligands, and two N atoms from two different bib linkers, exhibiting distorted single-capped octahedral coordination geometry. While Fe (2) is surrounded by six O atoms offered by five carboxylate oxygen atoms and one O^{2-}, showing a {FeO₆} octahedral coordination geometry.
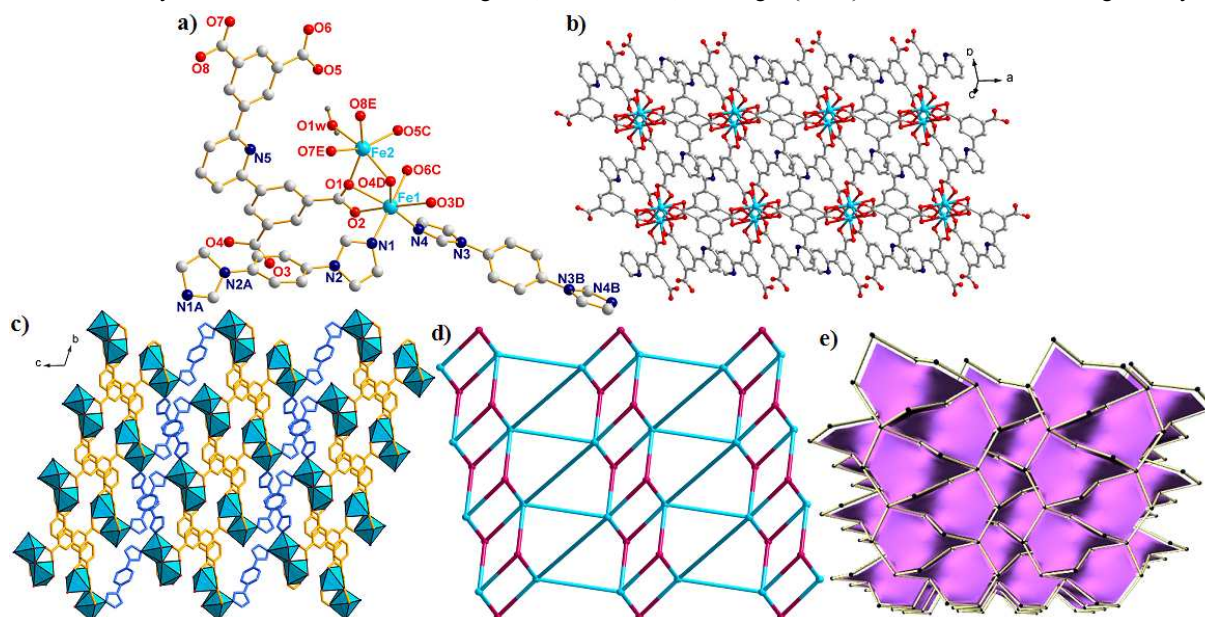
Figure 5. (a) Crystal structure of complex **5** (Symmetry codes: A: 2−x, 1−y, 2−z; B: 1−x, 3−y, 2−z; C: 1−x, 1−y, 1−z; D:−1+x, y, z; E: 1−x, −y, 1−z.). (b) The 2D [Fe₂(BDP)]ₙ network. (c) Schematic view of the 3D frameworks of **5** along a direction. (d) The novel 3D (4,6)–connected $(4^4\cdot6^{10}\cdot8)(4^4\cdot6^2)$ net of **5** (green spheres: {Fe₂(COO)₄} clusters based SBUs, red spheres: BDP^{4-} ligands). (e) Topological features of **5** displayed by tiling style.

Table 2 The detailed comparisons of complexes **1–5**.

Complex	Coord. Modes	$M(H_xBDP)_n$ Motifs	Dihedral Angles (°) of H_xBDP	Final Structure and Topology
1	Mode I	1D $[Cu(H_2BDP)]_n$ chain	18.9(5)/31.5(9)/18.9(5)	2D 4-connected $(4^4 \cdot 6^2)$-**sql** sheet
2	Mode II	2D $[Co_3(HBDP)_2]_n$ sheet	2.3(4)/23.5(6)/24.7(3)	3D (3,4,5)-connected $(4^2 \cdot 6^4 \cdot 7^3 \cdot 9)_2(6^2 \cdot 7)_2(6^4 \cdot 7 \cdot 8)$ net
3	Mode III	3D $[Co_2(BDP)]_n$ net	26.4(1)/10.6(6)/22.8(4)	3D (4,4,8)-connected $(3 \cdot 4^2 \cdot 5^2 \cdot 6)_4(3^2 \cdot 4^4 \cdot 5^4 \cdot 6^4 \cdot 7^2 \cdot 8^6 \cdot 9^5 \cdot 10)$ net
4	Mode IV	2D $[Mn_2(BDP)]_n$ sheet	7.1(5)/13.7(9)/7.1(5)	3D (4,8)-connected $(6^3)(6^9 \cdot 8)$-**gra** net
5	Mode V	2D $[Fe_2(BDP)]_n$ bilayer	31.5(2)/3.5(7)/34.9(5)	3D (4,6)-connected $(4^4 \cdot 6^{10} \cdot 8)(4^4 \cdot 6^2)$ (4,8) net

The ligand of H_4BDP is completely deprotonated and acts as μ_7 node to coordinate seven Fe^{II} ions through four carboxylate groups, which adopt $(\kappa^1\text{-}\kappa^2)\text{-}\mu_2$, $(\kappa^1\text{-}\kappa^1)\text{-}\mu_2$, and $(\kappa^1\text{-}\kappa^1)\text{-}\mu_1$ coordination modes (Mode V). Two Fe^{II} ions are coordinated by two $(\kappa^1\text{-}\kappa^2)\text{-}\mu_2$ and one $(\kappa^1\text{-}\kappa^1)\text{-}\mu_2$ carboxylate groups to form a binuclear $\{Fe_2(COO)_4\}$ binuclear SBUs, which are linked by BDP^{4-} ligands to generate a 2D $[Fe_2(BDP)]_n$ bilayer (Fig. 5b), which is linked by bib ligands to generate an unprecedented (4,6)-connected net with the Schläfli symbol of $(4^4 \cdot 6^{10} \cdot 8)(4^4 \cdot 6^2)$ by denoting the $\{Fe_2(COO)_4\}$ binuclear SBUs to 6−connected nodes and BDP^{4-} ligands to 4−connected nodes, respectively (Fig. 5d and 5e).
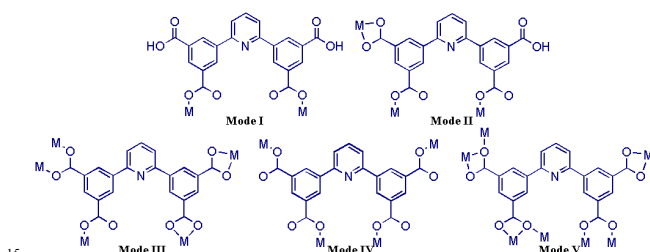
Scheme 2. The coordination modes of H_4BDP in complexes **1-5**.
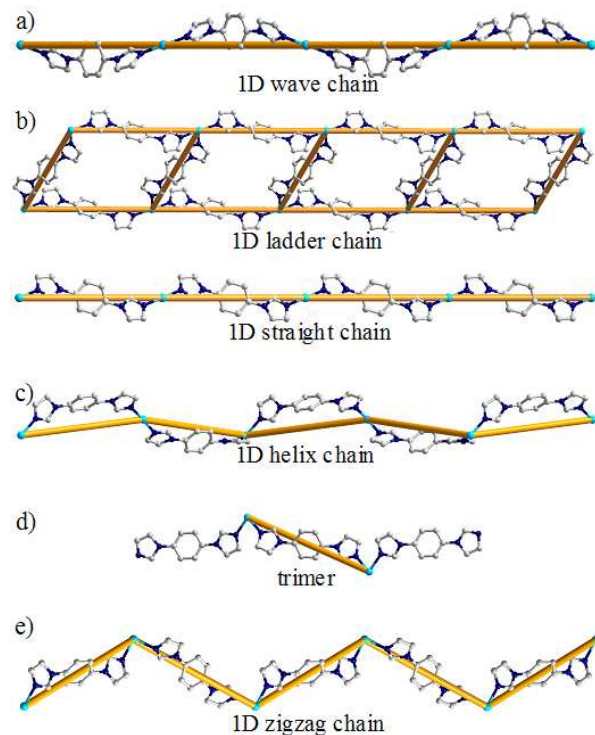
Scheme 3. The comparison of the structural motifs of $M(bib)_n$ in complexes **1-5** (a for **1**, b for **2**, c for **3**, d for **4**, and e for **5**).

Syntheses and Structural Comparison. As shown in Scheme 1, complexes **1-5** were successfully self-assembled by systematically selecting and tuning the ratios of mixed solvent and pH values. It is worth mentioning that during our exploration of the synthetic pathways, it has been found that mixed solvent plays a key on the construction of new coordination frameworks. Although pure H_2O, DMF, and CH_3OH were employed as reaction solvent with different pH values adjusted by NaOH or organic base under different temperature (120~180 °C), no suitable crystals for X-ray diffraction analysis were obtained, usually leading to the isolation of a powder product or the crystals of H_4BDP. From the synthetic comparison of complexes **2** and **3**, it is clear that only the alkaline reaction environments could lead to the complete depronation of polycarboxylate ligand. The differences in these synthetic processes of **2-5** are the ratios of the mixed solvent DMF/H_2O: a ratio of 12:2 for complex **3**, 6:3 for complex **4**, and 14:2 for complex **5**, which maybe due to that the crystal growth for different metal ions needs different concentration.

As shown in Schemes of 2 and 3 and Table 2, H_4BDP/BDP ligands took on five different coordination modes in the five CPs, and thus resulted in five diverse MOFs, which exhibit a systematic variation of architectures. It is worthy to note that the five CPs based on four metal cations were synthesized from completely different reaction conditions, including pH, ration of solvents, temperature. This proved that predicting and accurately controlling the framework array is a considerable challenge at this stage, due to that the crystal growth is influenced by many subtle intrinsic and external parameters. Among the five CPs, BDP^{4-} in **5** exhibits the largest coordination number of μ_7, maybe due to the factors of the metal cation (Fe^{II}), the high temperature (170 °C), and pH (NaOH). As for the auxiliary ligand of bib, it adopts *cis*- coordination mode in **1** and **3**, whereas, trans- in **2**, **4**, and **5**, which is more favourable to the crystal growth than bipyridine ligands. The obtained structural research in this report also proved our anticipation that H_4BDP is one interesting candidate to build CPs, due to that it possesses the followed characters: (i) the four carboxyl groups enrich the coordination modes, which can further lead to diverse interesting structures, (ii) the easy rotation through C-C single bonds among three aromatic rings permit it to link more metal cations, shown in Table 2.

Thermal Analyses. The thermogravimetric (TG) analyses were performed in N_2 atmosphere on polycrystalline samples of complex **1–5** and the TG curves are shown in Fig. S8. For complex **1**, the TGA curve shows the weight loss of 5.23 % at about 110 °C, which corresponds to the loss of lattice water molecules (5.05 %). And then the networks remains stable until the temperature up to 375 °C, finally the complex was pyrolyzed with a result of thermal decomposition. For complex **2**, the first weight loss of 7.67 % in the range of 80-140 °C can be attributed to the release of coordinated and lattice water molecules (7.31 %). And the sencond weight loss at about 380 °C corresponds to the loss of the organic ligands, finally given some unknown powder.

There are also two main stages of weight loss in the sample collapses of complex **3**. The first weight loss of 2.17 % below 100 °C is ascribed to the release of lattice water molecules (1.88 %). And then the frameworks can be exist stably below 380
5 °C. Above this temperature, the net collapsed with both the BDP^{4-} and bib released. In the case of complex **4**, the weight loss of 6.41 % from 70 to 150°C is attributed to the loss of coordinated and lattice water molecules (calc. 5.92 %). The weight loss corresponding to the release of organic ligands starts
10 at 340°C with a result of thermal decomposition. For complex **5**, the coordinated and lattice water molecules loss around 100°C, with the weight loss of 4.96 % (calc. 4.73 %). And then the organic pillars of the frameworks begin to pyrolyze when the temperature up to 410 °C, finally given a result of thermal
15 decomposition.

Magnetic Properties. The single crystal X-ray diffraction analyses reveal that different binuclear transition metal clusters in complexes **3-5**, which may be showing excellent magnetic properties. Thus, the variable-temperature magnetic susceptibility
20 measurements of complexes **3-5** were investeated and performed in Fig. 6-8.

For complex **3**, the $\chi_M T$ value at room temperature is 5.18 cm^3 K mol^{-1}, is much larger than the value expected for two isolated high-spin Co^{II} ions (3.75 cm^3 K mol^{-1}), which mainly due to the
25 orbitally nondegenerate ground term of octahedral Co^{II} ions. With the temperature decreasing, the $\chi_M T$ value decreases continuously to 1.92 cm^3 K mol^{-1} at about 2K. The temperature dependence χ_M followed the Curie-Weiss law $\chi_M = C/(T-\theta)$ with C= 5.46 cm^3 K mol^{-1}, $\theta = -22.47$ K (Fig. 6, inserted figure). And
30 the negative value of θ also indicates the presence of an antiferromagnetic interaction exist between two Co^{II} ions of the {Co$_2$(COO)$_2$} clusters based SBUs, similar with the reported ones. The susceptibility data were fit with an isotropic dimeric mode of the S = 3/2 spin, and the leastsquares analysis gives g =
35 2.05, $J = -0.12$ cm^{-1}, $R = -9.1 \times 10^{-4}$. The fitting result is comparable with the reported Co^{II} dimmers. [19a-c]

For complex **4**, the $\chi_M T$ value at room temperature is 4.55 cm^3 K mol^{-1}, much lower than that for two spin-only magnetically isolated Mn^{II} ions (8.75 cm^3 K mol^{-1}), which can be attributed to
40 antiferromagnetic interactions between Mn^{II} ions. With the temperature decreasing, the $\chi_M T$ value decreases continuously to 2.05 cm^3 K mol^{-1} at about 2K. The temperature dependence χ_M followed the Curie-Weiss law $\chi_M = C/(T-\theta)$ with C= 4.74 cm^3 K mol^{-1}, $\theta = -14.85$ K (Fig. 7, inserted figure), similar with the
45 above reported ones. The negative value of θ also indicates the presence of an antiferromagnetic interaction exist between the adjacent Mn^{II} ions. The susceptibility data were fit with a dimeric mode, and the leastsquares analysis gives g = 2.03, $J = -0.22$ cm^{-1}, $R = -3.7 \times 10^{-4}$. The fitting result is comparable with the
50 reported other Mn^{II} dimmers. [19d,e]

The magnetic susceptibilities data of complex **5** were collected in the range of 2-300K under an applied field of 1 kOe. The value of $\chi_M T$ value of complex **5** is 4.36 cm^3 K mol^{-1} at 300 K. And then the susceptibility curve ($\chi_M T$) decreases monotonically when
55 cooling, reaching the lowest value of 0.72 cm^3 K mol^{-1} at 2K with the molar susceptibility χ_M showing a maximum. The temperature dependence χ_M^{-1}-T is nonlinear, the χ_M^{-1} value at 300 K is 68.85 mol cm^{-3}, and with the temperature decreasing, the χ_M^{-1}

value decreases to 2.76 mol cm^{-3} at 2 K. So an
60 antiferromagnetic coupling can be expected between Fe^{II} ions. The susceptibility data were fit with the dimeric mode (S = 2), and the leastsquares analysis gives g = 2.859, $J = -1.54$ cm^{-1}, $R = -3.4 \times 10^{-3}$, similar to other reported Fe^{II} dimmers. [20]

In short, the magnetic properties are mainly derived from the
65 binuclear units, (Co$_2$(COO)$_2$) SBUs in **3**, {Mn$_2$(μ_2-H$_2$O)} SBUs in **4**, and {Fe$_2$(COO)$_4$} SBUs in **5**.
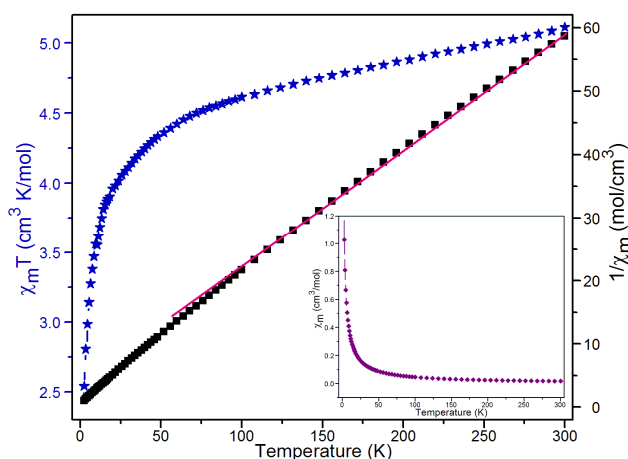
Figure 6. The temperature dependence of magnetic susceptibility of **3** under a static field of 1000 Oe.
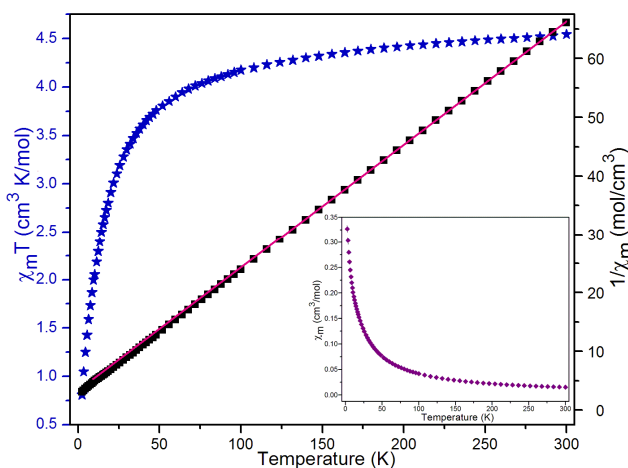
70 **Figure 7.** The temperature dependence of magnetic susceptibility of **4** under a static field of 1000 Oe.
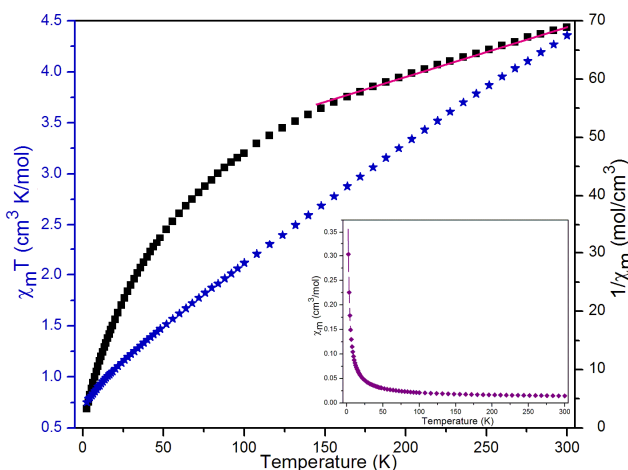
Figure 8. The temperature dependence of magnetic susceptibility of **5** under a static field of 1000 Oe.

Conclusions

In summary, we successfully report a synthetic method of coordination polymers in a mixed solvent mixture through solvothermal reactions with the variable ratio of mixed solvent, or even different mixture. Using this method, five multi-dimensional coordination polymers have been successfully fabricated from the H_4BDP and bib ligand, which represents the most complicated system that can be monitored by the ratio of the mixed solvent so far. This study broadens the exploration of the synthetic strategy on CPs construction. Magnetic measurements reveal that the antiferromagnetic properties exist between the two nearest neighboring cations in complexes **3**-**5**.

Notes

The authors declare no competing financial interest.

References

1. (a) T. R. Cook, Y. R. Zheng and P. J. Stang, *J. Chem. Rev.*, 2013, **113**, 734; (b) G. Férey and C. Serre, *Chem. Soc. Rev.*, 2009, **38**, 1380; (c) M. Kim, J. F. Cahill, H. Fei, K. A. Prather and S. M. Cohen, *J. Am. Chem. Soc.*, 2012, **134**, 18082; (d) D. S. Li, Y. P. Wu, J. Zhao, J. Zhang and J. Y. Lu, *Coord. Chem. Rev.*, 2014, **261**, 1; (e) Z. Hao, G. Yang, X. Song, M. Zhu, X. Meng, S. Zhao and H. Zhang, *J. Mater. Chem. A,* 2014, **2**, 237; (f) X. Wan, F. Jiang, L. Chen, M. Wu, M. Zhang, J. Pan, K. Su, Y. Yang and M. Hong, *Cryst. Growth Des.*, 2015, **15**, 1481.

2. (a) E. D. Bloch, W. L. Queen, R. Krishna, J. M. Zadrozny, C. M. Brown and J. R. Long, *Science*, 2012, **335**, 1606; (b) S. Chen, R. Shang, K. L. Hu, Z. M. Wang and S. Gao, *Inong. Chem. Front.*, 2014, **1**, 83; (c) X. T. Zhang, D. Sun, B. Li, L. M. Fan, B. Li and P. H. Wei, *Cryst. Growth Des.*, 2012, **12**, 3845; (d) W. Liu, X. Bao, L. L. Mao, J. Tucek, R. Zboril, J. L. Liu, F. S. Guo, Z. P. Ni and M. L. Tong, *Chem. Commun.*, 2014, **50**, 4059; (e) Z. Hao, X. Song, M. Zhu, X. Meng, S. Zhao, S. Su, W. Yang, S. Song and H. Zhang, *J. Mater. Chem. A,* 2013, **1**, 11043.

3. (a) B. Liu, W. P. Wu, L. Hou and Y. Y. Wang, *Chem. Commun.*, 2014, **50**, 8731; (b) J. B. Lin, W. Xue, B. Y. Wang, J. Tao, W. X. Zhang, J. P. Zhang and X. M. Chen, *Inorg. Chem.*, 2012, **51**, 9423; (c) X. Zhang, L. Fan, Z. Zhang, Y. Ding, W. Fan and X. Zhao, *Dalton Trans.*, 2013, **42**, 16562; (d) J. L. Liu, Y. C. Chen, Y. Z. Zheng, W. Q. Lin, L. Ungur, W. Wernsdorfer, L. F. Chibotaru and M. L. Tong, *Chem. Sci.*, 2013, **4**, 3310; (e) D. S. Li, Y. P. Wu, P. Zhang, M. Du, J. Zhao, C. P. Li and Y. Y. Wang, *Cryst. Growth Des.*, 2010, **10**, 203; (f) Q. Zhang, H. Zhang, S. Zeng, D. Sun and C. Zhang, *Chem-Asian J.*, 2013, **8**, 1985.

4. (a) W. L. Leong and J. J.Vittal, *Chem. Rev.*, 2011, **111**, 688; (b) P. Yang, M. S. Wang, J. J. Shen, M. X. Li, Z. X. Wang, M. Shao and X. He, *Dalton Trans.,* 2014, **43**, 1460; (c) L. L. Han, T. P. Hu, J. S. Chen, Z. H. Li, X. P. Wang, Y. Q. Zhao, X. Y. Li and D. Sun, *Dalton Trans.,* 2014, **43**, 8774; (d) W. Shi, S. Song and H. Zhang, *Chem. Soc. Rev.*, 2013, **42**, 5714; (e) K. Wang, S. Zeng, H. Wang, J. Dou and J. Jiang, *Inong. Chem. Front.*, 2014, **1**, 167.

5. (a) T. Liu, S. Wang, J. Lu, J. Dou, M. Niu, D. Li and J. Bai, *CrystEngComm*, 2013, **15**, 5476; (b) Y. Q. Chen, S. J. Liu, Y. W. Li, G. R. Li, K. H. He, Z. Chang and X. H. B, *CrystEngComm*, 2013, **15**, 1613; (c) L. Liu, X. Lv, L. Zhang, L. Guo, J. Wu, H. Hou and Y. Fan, *CrystEngComm*, 2014, **16**, 8736; (d) U. J. Williams, B. D. Mahoney, A. J. Lewis, P. T. DeGregorio, P. J. Carroll and E. J. Schelter, *Inorg. Chem.*, 2013, **52**, 4142; (e) K. Su, F. Jiang, J. Qian, L. Chen, J. Pang, S. M. Bawaked, M. Mokhtar, S. A. Al-Thabaiti and M. Hong, *Inorg. Chem.,* 2015, **54**, 3183.

6. (a) L. Fan, X. Zhang, D. Li, D. Sun, W. Zhang and J. Dou, *CrystEngComm*, 2013, **15**, 349; (b) X. Chang, J. Qin, M. Han, L. Ma and L. Wang, *CrystEngComm*, 2014, **16**, 870; (c) X. H. Chang, Y. Zhao, M. L. Han, L. F. Ma and L. Y. Wang, *CrystEngComm*, 2014, **16**, 6417; (d) L. P. Xue, C. X. Chang, S. H. Li, L. F. Ma and L. Y. Wang, *Dalton Trans.,* 2014, **43**, 7219; (e) M. L. Han, X. C. Chang, X. Feng, L. F. Ma and L. Y. Wang, *CrystEngComm*, 2014, **16**, 1687; (f) L. L. Liu, C. X. Yu, J. Sun, P. P. Meng, F. J. Ma, J. M. Du and L. F. Ma, *Dalton Trans.,* 2014, **43**, 2915.

7. (a) G. L. Liu and H. Liu, *CrystEngComm*, 2013, **15**, 6870; (b) C. Zhan, C. Zou, G. Q. Kong and C. D. Wu, *Cryst. Growth Des.*, 2013, **13**, 1429; (c) J. J. Wang, T. T. Wang, L. Tang, X. Y. Hou, L. J. Gao, F. Fu and M. L. Zhang, *J. Coord. Chem.*, 2013, **66**, 3979; (d) X. Chang, Y. Zhao, M. Han, L. Ma and L. Wang, *CrystEngComm*, 2014, **16**, 6417; (e) D. S. Li, X. J. Ke, J. Zhao, M. Du, K. Zou, Q. F. He and C. Li, *CrystEngComm*, 2011, **13**, 3355; (f) M. Meng, D. C. Zhong and T. B. Lu, *CrystEngComm*, 2011, **13**, 6794.

8. (a) R. E. Osta, M. Frigoli, J. Marrot, N. Guillou, H. Chevreau, R. I. Walton and F. Millange, *Chem. Comm.*, 2012, **48**, 10639; (b) J. Zhao, D. S. Li, X. J. Ke, B. Liu, K. Zou and H. M. Hu, *Dalton Trans.,* 2012, **41**, 2560; (c) W. Liu, L. Ye, X. Liu, L. Yuan, J. Jiang and C. Yan, *CrystEngComm*, 2008, **10**, 1395; (d) M. Yan, F. Jiang, Q. Chen, Y. Zhou, R. Feng, K. Xiong and C. Hong, *CrystEngComm*, 2011, **13**, 3971.

9. (a) L. Qin, M. Zhang, Q. Yang, Y. Li and H. Zheng, *Cryst. Growth Des.*, 2013, **13**, 5045; (b) Q. Ma, X. Feng, W. Cao, H. Wang and J. Jiang, *CrystEngComm*, 2013, **15**, 10383; (c) L. Zhang, J. Guo, Q. Meng, R. Wang and D. Sun, *CrystEngComm*, 2013, **15**, 9578; (d) H. R. Fu, F. Wang and J. Zhang, *Dalton Trans.,* 2014, **43**, 4668; (e) H. L. Jia, Z. Shi, Q. F. Yang, J. H. Yu and J. Q. Xu, *Dalton Trans.,* 2014, **43**, 5806; (e) X. Zhang, L. Fan, W. Zhang, W. Fan, L. Sun and X. Zhao, *CrystEngComm*, 2014, **16**, 3203; (f) L. Fan, W. Fan, B. Li, X. Liu, X. Zhao and X. Zhang, *Dalton Trans.*, 2015, **44**, 2380.

10. (a) H. Deng, S. Grunder, K. E. Cordova, H. Furukawa, M. Hmadeh, F. Gandara, A. C. Whalley, Z. Liu, S. Asahina, H. Kazumori, M. O'Keefee, O. Terasaki, J. F. Stoddart and O. M. Yaghi, *Science*, 2012, **336**, 1018; (b) L. F. Ma, Z. Z. Shi, F. F. Li, J. Zhang and L. Y. Wang, *New J. Chem.*, 2015, **39**, 810; (c) X. C. Yi, M. X. Huang, Y. Qi and E. Q. Gao, *Dalton Trans.,* 2014, **43**, 3691; (d) J. Yang, X. Wang, F. Dai, L. Zhang, R. Wang and D. Sun, *Inorg. Chem.,* 2014, **53**, 10649; (e) H. Jia, Y. Li, Z. Xiong, C. Wang and G. Li, *Dalton Trans.,* 2014, **43**, 3704; (f) J. Cui, Y. Li, Z. Guo and H. Zheng, *Chem. Commun.*, 2013, **49**, 555; (g) J. H. Qin, L. F. Ma, Y. Hu and L. Y. Wang, *CrystEngComm*, 2012, **14**, 2891.

11. (a) Y. Mu, G. Han, S. Ji, H. Hou and Y. Fan, *CrystEngComm*, 2011,**13**, 5943; (b) Fan, W. Fan, W. Song, G. Liu, X. Zhang and X. Zhao, *CrystEngComm*, 2014, **16**, 9191; (c) X. Zhang, L. Fan, Z. Sun, W. Zhang, W. Fan, L. Sun and X. Zhao, *CrystEngComm*, 2013, **15**, 4910; (d) X. Q. Song, Y. K. Lei, X. R. Wang, M. M. Zhao, Y. Q. Peng and G. Q. Cheng, *J. Solid State Chem.*, 2014, **210**, 178; (e) H. Y. Lin, J. Luan, X. L. Wang, J. W. Zhang, G. C. Liu and A. X. Tian, *RSC Adv.*, 2014, **4**, 62430.

12. (a) X. H. Chang, J. H. Qin, M. L. Han, L. F. Ma and L. Y. Wang, *CrystEngComm*, 2014, **16**, 8720; (b) W. Yang, C. Yang, Q. Ma, C. Li, H. Wang and J. Jiang, *CrystEngComm*, 2014, **16**, 4554; (c) T. Wu, Y. J. Lin and G. X. Jin, *Dalton Trans.*, 2014, **42**, 82; (d) F. Y. Yi, S. Dang, W. Yan and Z. M. Sun, *CrystEngComm*, 2013, **15**, 8320; (e) X. Y. Dong, R. Wang, J. B. Li, S. Q. Zang, H. W. Hou and T. C. K. Mark, *Chem. Commun.*, 2013, **49**, 10590.

13. (a) Y. W. Li, D. C. Li, J. Xu, H. G. Hao, S. N. Wang, J. M. Dou, T. L. Hu and X. H. Bu, *Dalton Trans.,* 2014, **43**, 15708; (b) T. Cao, Y. Peng, T. Liu, S. Wang, J. Dou, Y. Li, C. Zhou, D. Li and J. Bai, *CrystEngComm*, 2014, **16**, 10658; (c) L. Zhang, J. Guo, Q. Meng, R. Wang and D. Sun, *CrystEngComm*, 2013, **15**, 9578; (d) Z. H. Yan, X. W. Zhang, H. Pang, Y. Zhang, D. Sun and L. Wang, *RSC Adv.*, 2014, **4**, 53608; (e) L. Fan, W. Fan, B. Li, X. Liu, X. Zhao and X. Zhang, *RSC Adv.*, 2015, **5**, 14897; (f) L. L. Liu, C. X. Yu, Y. R. Li,

J. J. Han, F. J. Ma and L. F. Ma, *CrystEngComm*, 2015 ,**17**, 653; (g) X. Feng, Y. Q. Feng, J. J. Chen, S. W. Ng, L. Y. Wang and J. Z. Guo, *Dalton Trans.*, 2015, **44**, 804.

14. (a) X. T. Zhang, L. M. Fan, X. Zhao, D. Sun, D. C. Li and J. M. Dou, *CrystEngComm*, 2012, **14**, 2053; (b) L. Fan, Y. Gao, G. Liu, W. Fan, W. Song, L. Sun, X. Zhao and X. Zhang, *CrystEngComm*, 2014, **16**, 7649; (c) L. Fan, X. Zhang, W. Zhang, Y. Ding, W. Fan, L. Sun, Y. Pang and X. Zhao, *Dalton Trans.,* 2014, **43**, 6701; (d) L. Fan, W. Fan, W. Song, L. Sun, X. Zhao and X. Zhang, *Dalton Trans.,* 2014, **43**, 15979.

15. (a) L. L. Liu, C. X. Yu, F. J. Ma, Y. R. Li, J. J. Han, L. Lin and J. F. Ma, *Dalton Trans.*, 2015, **44**, 1636; (b) Z. Wu, W. Sun, Y. Chai, W. Zhao, H. Wu, T. Shi and X. Yang, *CrystEngComm*, 2014, **16**, 406; (c) X. H. Chang, Y. Zhao, M. L. Han, L. F. Ma and L. Y. Wang, *CrystEngComm*, 2014, **16**, 6417; (d) F. Guo, B. Zhu, M. Liu, X. Zhang, J. Zhang and J. Zhao, *CrystEngComm*, 2013, **15**, 6191; (e) L. Chen, L. Zhang, S. L. Li, Y. Q. Qiu, K. Z. Shao, X. L. Wang and Z. M. Su, *CrystEngComm*, 2013, **15**, 8214; (f) F. L. Hu, Y. Mi, Y. Q. Guo, L. G. Zhu, S. L. Yang, H. Wei and J. P. Lang, *CrystEngComm*, 2013, **15**, 9553; (g) X. Zhang, L. Fan, W. Song, W. Fan, L. Sun and X. Zhao, *RSC Adv.*, 2014, **4**, 30274; (h) L. Fan, W. Fan, B. Li, X. Zhao and X. Zhang, *RSC Adv.*, 2015, **5**, 39854.

16. (a) G. Mehlana, S. A. Bourne, G. Ramon and L. Ohrstrom, *Cryst. Growth Des.*, 2013, **13**, 633; (b) L. Fan, X. Zhang, W. Zhang, Y. Ding, L. Sun, W. Fan and X. Zhao, *CrystEngComm*, 2014, **16**, 2144; (c) X. T. Zhang, L. M. Fan, Z. Sun, W. Zhang, D. C. Li, J. M. Dou and L. Han, *Cryst. Growth Des.*, 2013, **13**, 792; (d) L. Fan, X. Zhang, Z. Sun, W. Zhang, Y. Ding, W. Fan, L. Sun, X. Zhao and H. Lei, *Cryst. Growth Des.*, 2013, **13**, 2462.

17. (a) G. M. Sheldrick, *SHELXTL*, version 5.1; Bruker Analytical X-ray Instruments Inc.: Madison, WI, 1998. (b) G. M. Sheldrick, *SHELX-97*, PC Version; University of Gottingen: Gottingen, Germany, 1997.

18. (a) V. A. Blatov, A. P. Shevchenko and V. N. Serezhkin, *J. Appl. Crystallogr.*, 2000, **33**, 1193; (b) The network topology was evaluated by the program "TOPOS-4.0", see: http://www.topos.ssu.samara.ru. (c) V. A. Blatov, M. O'Keeffe and D. M. Proserpio, *CrystEngComm*, 2010, **12**, 44.

19. (a) F. L. Hu, W. Wu, P. Liang, Y. Q. Gu, L. G. Zhu, H. Wei and J. [. Lang, *Cryst. Growth Des.*, 2013, **13**, 5058; (b) Q. Q. Li, Y. F. Kang, C. Y. Ren, G. P. Yang, Q. Liu, P. Liu and Y. Y. Wang, *CrystEngComm*, 2015, **17**, 775; (c) M. L. Han, Y. P. Duan, D. S. Li, H. B. Wang, J. Zhao and Y. Y. Wang, *Dalton Trans.,* 2014, **43**, 15450; (d) L. F. Ma, M. L. Han, J. H. Qin, L. Y. Wang and M. Du, *Inorg. Chem.*, 2012, **51**, 9431.

20. (a) G. Lemercier, E. Mulliez, C. Brouca-Cabarrecq, F. Dahan and J. Tuchagues, *Inorg. Chem.*, 2004, **43**, 2105; (b) W. T. Liu, J. Y. Li, Z. P. Ni, X. Bao, Y. C. Ou, J. D. Leng, J. L. Liu and M. L. Tong, *Cryst. Growth Des.*, 2012, **12**, 1482; (c) X. Bao, W. Liu, L. L. Mao, S. D. Jiang, J. L. Liu, Y. C. Chen and M. L. Tong, *Inorg. Chem.*, 2013, **52**, 6233; (d) Y. W. Li, J. P. Zhao, L. F. Wang and X. H. Bu, *CrystEngComm*, 2011, **13**, 6002.